Nuclear Engineering and Technology 52 (2020) 2803–2811

Contents lists available at ScienceDirect

Nuclear Engineering and Technology

journal homepage: www.elsevier.com/locate/net

Original Article

CFD study of the PTS experiment in ROCOM test facility

Zoran Čarija [a, b, *], Fran Ledić [a], Ante Sikirica [b, a], Bojan Niceno [c]

[a] Faculty of Engineering, University of Rijeka, Vukovarska 58, 51000, Rijeka, Croatia
[b] Center for Advanced Computing and Modelling, University of Rijeka, Radmile Matejčić 2, 51000, Rijeka, Croatia
[c] Paul Scherrer Institute, Forschungsstrasse 111, 5232, Villigen PSI, Switzerland

ARTICLE INFO

Article history:
Received 12 January 2020
Received in revised form
17 April 2020
Accepted 1 June 2020
Available online 5 June 2020

Keywords:
ROCOM
CFD
Turbulent mixing

ABSTRACT

With the aging of nuclear reactors, embrittlement of the reactor pressure vessel (RPV) steel, as a consequence of routine operations, is highly probable. To ensure operational integrity and safety, prediction and mitigation of compromising damage, brought on by pressurized thermal shock (PTS) following an emergency procedure, is of utmost importance. Computational fluid dynamics (CFD) codes can be employed to predict these events and have therefore been an acceptable method for such assessments. In this paper, CFD simulations of a density driven ECC state in the ROCOM facility are analyzed. Obtained numerical results are validated with the experimental measurements. Considerable attention is attributed to the boundary conditions and their influence, specifically outlet definitions, in order to determine and adequately replicate the non-active pumps in the facility. Consequent analyses focused on initial conditions as well as on the temporal discretization and inner iterations. Disparities due to different turbulent modelling approaches are investigated for standard RANS models. Based on observed trends for different cases, a definitive simulation setup has been established, results of which have been ultimately compared to the measurements.

1. Introduction

During routine nuclear reactor operations mechanical failings such as stuck valves, ruptures or line breaks can result in loss of coolant accidents (LOCA). Once a LOCA is detected, an emergency procedure triggers the emergency core cooling (ECC) system which injects cooler, borated water, into the reactor cooling loop. Water introduced during ECC procedures acts as a neutron poison, maximizing neutron absorption and ensuring reactor shutdown while maintaining the reactor circulation and compensating for the potentially incurred leakage.

Temperature-driven differences in physical properties of the injected and circulating water in the reactor (coolant water), can, at lower velocities, result in partial mixing of the coolants and lead to buoyancy driven thermal stratification (TS) which manifests as temperature-based coolant lamination. In case of such an event, large temperature gradients can occur on the reactor pressure vessel (RPV) causing high thermal stresses which can potentially damage the RPV, particularly in the downcomer area, where, according to experimental values [1], gradients are the highest. In general, routine exposure to varying thermal stresses, including low intensity ones, leads to the accumulation of fatigue [2]. Combined with the neutron radiation incurred embrittlement of the material, rapid temperature change and high temperature gradients can cause pressurized thermal shock (PTS), a damaging occurrence that can results in the eventual failure of the RPV. This is particularly significant for older reactors where aging and years of exposure to TS and neutron radiation increase the risk of loss of structural integrity. In view of this, mixing and overall flow in TS conditions has been the focus of research for the past thirty years.

Mixing of the coolants in the reactor cannot be assumed as homogeneous (i.e. ideal mixing), as demonstrated by Grundmann and Rohde [3], and therefore requires comprehensive experimental examination [4,5] in order to develop prediction models which ensure functionality and safety. Seeing as the assessment of potentially hazardous scenarios is not possible in a working reactor, experimental investigations are routinely conducted in experimental facilities which enable the reproduction of the flow patterns and mixing. Through the FLOMIX-R project [1,6], buoyancy driven mixing and momentum controlled mixing in highly turbulent flows, fundamental mixing phenomena within the nuclear reactor, have been thoroughly investigated in multiple testing facilities.

* Corresponding author. Faculty of Engineering, University of Rijeka, Vukovarska 58, 51000, Rijeka, Croatia.
E-mail address: zcarija@riteh.hr (Z. Čarija).

https://doi.org/10.1016/j.net.2020.06.002

Obtained experimental data for various test cases has subsequently been employed to validate CFD codes. Presently, this data is commonly used for mixing studies as well as general CFD validation. Experiments describing ECC water propagation and slug transport towards the core via natural circulation have been reported by Kliem et al. [7]. Subsequent works by Kliem et al. [8] followed by Prasser and Kliem [9] further expanded on this, introducing new cases and experimental measurements.

Complex mixing phenomena in nuclear reactors, in the wake of computing advancements, has been increasingly investigated using CFD. This risk-free and inexpensive approach relies on numerical algorithms to model flow characteristics. Studies by Prasser et al. [10] and Rohde et al. [11] conducted validation based on currently accessible experimental data using Reynolds-averaged Navier-Stokes (RANS) approach to turbulence modelling. FLOMIX-R project [6] provided detailed CFD code validation using k-ε, k-ω and RSM turbulence models. Schaffrath et al. [12] replicated ROCOM experiment T6655 21 using CFD code and various two-equation turbulent models. Study has shown that the experimental data and numerical results can differ by 5%. However, these findings have been deemed acceptable and have been confirmed by Moretti et al. [13]. Authors concluded that k-ε and SST k-ω turbulent models have the ability to adequately model mixing and show overall good agreement with the experimental data, despite some discrepancies, similarly to Refs. [6,12]. Works by Hohne et al. [14,15] additionally included LES analyses. These results provided marginal improvements with errors attributed to the numerical grid. Paper by Labois et al. [16] introduced a novel CFD/CMFD approach which utilizes a solid level set function in order to resolve complex flow in the ROCOM facility. Presented results were in acceptable ranges. Cho and Yoon [17] investigated the applicability of CPUID code on ROCOM 21 test case with underpredicted results. Studies by Moretti [18] and subsequently by Boumaza et al. [19] assessed the effect of uniform and non-uniform inlet velocity profiles on the flow field in the ROCOM facility. Both authors concluded that non-uniform, specifically power-law inlet profile, leads to better flow predictions in the downcomer. Feng et al. [20] and Hohne et al. [21] have conducted LES analyses for ROCOM benchmark cases with observations similar to Refs. [15]. Recently, Puragliesi [22] analyzed the applicability of unsteady RANS models for use in main steam line break and loss of off-site power scenarios described in the NEA/OECD PKL2 project. The author concluded that attained numerical errors can be directly attributed to inadequacy of RANS models and suggested the use of scale resolving simulations.

Assessing the quality of CFD codes within the nuclear research community is one of the mandates of the International Atomic Energy Agency's (IAEA) CRP on CFD use in nuclear power plant design. Consequently, in this study, ROCOM D10m10 experimental measurements will be used as a baseline for the assessment of the use of CFD for PTS scenario simulations. The main goal is to investigate the influence of different turbulent models, as well as the influence of varying initial and boundary conditions on the solution. These results will be used to stress the importance of knowing the exact parameters of the simulated event and to show how dangerous misinterpretations can be.

2. Rossendorf coolant mixing model (ROCOM)

2.1. Experimental facility

In order to provide insight into coolant mixing within nuclear reactors, thus ensuring reactor structural and functional integrity, scaled experimental facilities have been envisioned and constructed. Rossendorf ROCOM experimental facility is a quintessential facility, a scaled down perspex model of the primary circuit of a Konvoi-type PWR nuclear reactor [1]. Facility is utilized as a source of experimental data on mixing problems. ROCOM facility uses a linear scale of 1:5 with respect the original PWR reactor. Four coolant loops connect to an RPV mock-up; flow is realized through the cold legs (CL), ECC inlet nozzles, the downcomer (DC), core and finally hot legs (HL). The flow in the loops is scaled according to the transit time of the coolant through the reactor model [10]. Consequently, coolant flow and mixing can be analyzed in different sections and for varying flow conditions including natural and forced convection.

Apart from the core, geometric relations are preserved in full throughout the model. The core itself is modeled with a set of tubes which are able to attain hydraulic resistance with the appropriate Euler number [15]. Flow patterns and overall mixing results noted in the ROCOM facility can therefore be used to accurately describe events in an actual reactor. An overview of geometric parameters and generator specifics for the Konvoi reactor and ROCOM test facility is given in Table 1.

The ROCOM facility utilizes demineralized water at the room temperature as a coolant. As the model lacks heating elements, temperature-driven density and viscosity changes of the coolant in the real reactor are simulated using additives, mainly glucose. Applied properties of the solution are therefore defined as a function of the user defined scalar (UDS) that corresponds to the mixing scalar. Linear correlation is assumed for density whereas non-linearity of the viscosity is accounted for by curve fitting known data with respect to the UDS. Indicated properties are imparted through a user defined function. Tracer solution, usually sodium chloride, is used to monitor ECC water flow. It is injected with the water, slightly altering its conductivity. Conductivity is subsequently determined with wire-mesh electrical conductivity sensors. Sensor setup used in the D10M10 experiment, which is the focus of this study, consists of four mesh sensors placed at key positions. The reactor inlet sensor is clamped to the CL of Loop 1 (before entering the RPV) and records tracer concentration at the inlet. Two grids with 16 perpendicular electrodes provide 256 measurement positions [1]. In the upper downcomer (UDC) and lower downcomer (LDC) identical sensors with 64 radial fixing rods each and orifices for four circular electrode wires are used. Rods gather circumferential measurements and similarly offer 256 measurement positions [1]. Electrode arrangement integrated into the core support plate contains 15 transmitter and 15 receiver electrodes in a matrix that allows measurement of the tracer concentration for each individual fuel element [1]. Fig. 1 outlines the locations of the sensors in the ROCOM facility. Sensors provide a total of approximately 1000 measuring points, each collecting data at a frequency of 200 Hz. Sampling of the distribution of electrical conductivity over a specified cross section is achieved by monitoring the electrical current that passes across two isolated grids. Result is a two-dimensional matrix of local conductivity values which can be correlated with the tracer concentrations. Concentration of the injected water can thus be monitored through the change in conductivity given that the remaining coolant inside the ROCOM generator is demineralized water [1].

Flow within the facility is fully turbulent, even during the natural circulation, as evidenced by high Reynolds values [1,13]. This behavior is typical of the real reactor model as well. Consequently, transport of a monitored scalar is primarily dependent on the turbulent mixing whereas molecular diffusion plays a secondary role. In order to resolve the effects of the molecular diffusion in wall-bounded flows, sufficiently refined grid is required. As this would result in an unsuitably large numerical grid, this aspect has been modeled.

Electrical conductivity attained with the previously mentioned sensor setup is commonly expressed as a dimensionless mixing

Table 1
ROCOM model characteristics.

Parameter	Konvoi reactor	ROCOM model
Inner diameter of the pressure vessel/mm	5000	1000
Height of the pressure vessel/mm	Approx. 12,000	Approx. 2400
Inner diameter of the inlet nozzle/mm	750	150
Width of the downcomer/mm	315	63
Coolant flow rate per loop/m^3h^{-1}	2300	185 (nom.) 350 (max)
Coolant inlet velocity/ms^{-1}	14.5	5.5 (max) 2.91 (nom.)
Velocity in the downcomer/ms^{-1}	5.5	2.1 (max) 1.1 (nom.)
Reynolds number in the inlet nozzle	$8.4\cdot10^7$	$8.3\cdot10^5$ (max) $4.4\cdot10^5$ (nom.)
Reynolds number in the downcomer	$2.7\cdot10^7$	$2.6\cdot10^5$ (max) $1.4\cdot10^5$ (nom.)
Relative Reynolds number	1	Approx. 100 (max) Approx. 190 (nom.)
Relative coolant travelling time	1	1 (nom.)

scalar. Since conductivity and concentration are proportional, mixing scalar in practical terms reflects the concentration at a measurement point. When water with different temperature is mixed, turbulent mixing processes that govern the mixing in the turbulent flow field are equal to those that drive the mixing based on concentration difference. Mixing scalar θ is defined as follows (1):

$$\theta_{x,y,z,t} = \frac{\sigma_{x,y,z,t} - \sigma_0}{\sigma_1 - \sigma_0} \cong \frac{T_{x,y,z,t} - T_0}{T_1 - T_0} \cong \frac{C_{B,x,y,z,t} - C_{B,0}}{C_{B,1} - C_{B,0}} \quad (1)$$

where σ represents measured electrical conductivity, T temperature and C_B boron concentration. Indices 0 and 1 denote unaffected (reference) and affected coolant in the reactor inlet nozzle. Noted linear relationship and overall analogy are true only for low viscosity solutions and passive scalars [18].

2.2. D10M10 PTS case

D10m10 experiment was one out of 21 buoyancy driven mixing experiments carried out in the ROCOM facility during the FLOMIX-R project [1]. These experiments assess mixing in the downcomer ensuing from density differences between primary loop inventory and the injected cold water. During the measurements flow in the system and density difference between the loop and ECC range from 0% to 15% and 0%–10% respectively, thus imitating natural circulation in the reactor [21]. Results acquired in these experiments are divided into two groups: momentum and density driven flows. Separation criteria is based on densimetric Froude number with $Fr = 1$ representing the critical value. Froude number is a dimensionless number measuring the ratio of inertial and gravitational forces and is defined as (2):

$$Fr = \sqrt{\frac{\rho w}{\Delta\rho g l}} \quad (2)$$

where w is the velocity, ρ density of the fluid, g gravitational acceleration, l characteristic length and $\Delta\rho$ density difference between the coolant inventory and the slug. For all density dominated flows $Fr < 0.85$, while for momentum dominated flows $Fr > 1.15$ [1,11].

Test case D10m10 employs a constant flow rate in a single loop equal to 10% of the nominal flow, with density difference of 10% between the loop and ECC water. Resulting Froude number equals $Fr = 0.85$, indicating this a density driven case, as can be seen in Fig. 2. Fluid used in the ECC injection is a glucose-water mixture with a density of 1096.7 kg/m^3. Velocity of the fluid in the CL of Loop 1 is 0.291 m/s. The ECC water is injected after 5 s. Injection period lasts 10 s with velocity set at 0.643 m/s. As per available data, remaining loops should be open and assigned pressure boundary conditions. An overview of experimental parameters for D10m10 case is given in Table 2 [1].

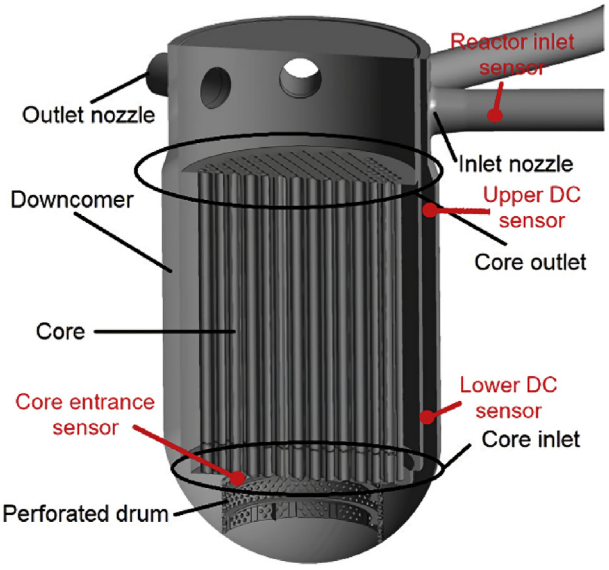

Fig. 1. ROCOM model and sensor locations.

3. Methodology

3.1. Numerical model

Numerical analysis has been conducted in ANSYS Fluent. Fluent is a finite-volume multipurpose CFD solver capable of solving both incompressible and compressible flow problems for arbitrary complex geometries [23]. Transient RANS simulations with two-equation linear eddy viscosity models (k-ε, k-ω) [24] and Reynolds stress model [24] are employed to resolve the flow in the ROCOM model. Simulations are completed using a segregated solver and second-order discretization schemes, or equivalents.

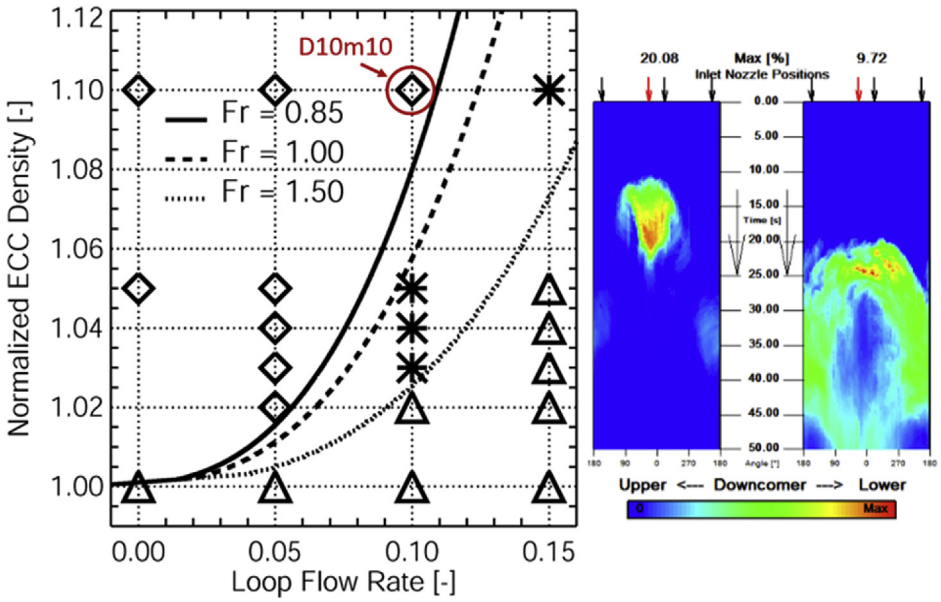

Fig. 2. Buoyancy driven mixing experiments [1] and tracer distributions in the UDC and LDC for D10m10 case [21].

Table 2
Experimental parameters for D10m10 case.

$\dot{V}_{ECC}$ / m^3s^{-1}	$V_{mag,ECC}$ / ms^{-1}	$\dot{V}_{Loop1}$ / m^3s^{-1}	$V_{mag,Loop1}$ / ms^{-1}	Density difference Loop1: ECC	Fr (downcomer)
3.6	0.643	18.5	0.291	1 : 1.1	0.85

3.2. Numerical grid

Numerical grid used in this study is generated using Pointwise Gridgen and contains $\approx 8.5 \cdot 10^6$ cells. The grid is hexahedral and utilizes both O-grid, U-grid and local density refinements so as to properly model complex geometry around the orifices, holes and curved areas. The perforated drum in the RPV is modeled without simplifications. Use of wall functions was necessary due to maintained dimensionless wall distance of around $y^+ \approx 30$. This choice was made deliberately as most of the mixing happens in the free stream. Proper resolution of the flow up to the wall (~20 cells in the boundary layer) would result in a larger cell count. It is reasonable to assume that purely hexahedral grids would provide significantly more accurate results. Since hexahedral block grids are more difficult to generate, recent studies employed tetrahedral [21] and polyhedral grids [22] which tend to be more sensitive to numerical diffusion.

3.3. Simulation settings

The main goal of this study is to ascertain the influence boundary conditions (BC) and initial conditions (IC) have on the mixing in the reactor. Furthermore, conventional numerical parameters used in CFD analyses, particularly turbulent models and transient settings (inner iterations and time step size), are assessed. Since the facility contains four distinct loops with corresponding pumps, only one of which is active at a time, it is sensible to simplify the calculations by employing a set of boundary conditions which accounts for all the flow modifiers in non-active loops. Principal assumption is that inactive pumps act as a hydraulic resistance. However, this assumption leads to uncertainties when analyzing complex flow problems and thus needs to be resolved. Therefore, three sets of boundary conditions have been identified with key difference being inactive loop treatment:

- Set 1 (BC_1): inactive loops HL's and CL's set as pressure outlets
- Set 2 (BC_2): flow through inactive loops CL's blocked with HL's set as outlets
- Set 3 (BC_3): all inactive loops set as closed with HL_1 set as the only outlet

Described boundary conditions have been implemented with two types of initial conditions:

- Cold start, i.e. initial fluid velocity in the domain is zero
- Warm start, i.e. initial velocity profile is based on a predetermined 20 s transient

Utilized IC's reflect the ambiguity in the experiment description [1] with regards to the way they were conducted. Furthermore, different RANS turbulent models have been evaluated:

- k-ε model
- k-ω model
- SST k- ω model
- Reynolds stress model

Relevant time step has been determined by gradually reducing the initial time step and monitoring the results until there has been no discernible change. Calculated time step t_s has subsequently been used as a reference in order to determine disparities inner iterations can introduce. Two distinct cases have been evaluated:

- $t_s = \frac{1}{64}s$, $2n$ inner iterations

- $t_s = \frac{1}{128}s$, $\leq n$ inner iterations

Validity of obtained numerical results is determined based on tracer concentrations. In total, seven distinct points located in CL_1, upper downcomer (UDC), lower downcomer (LDC) and the core inlet have been monitored, as per IAEA recommendations [25]. Furthermore, spatially averaged tracer concentrations in planes corresponding to the inlet sensor, upper downcomer, lower downcomer and the core inlet sensor have been tracked. Locations of points and planes used for data comparison are shown in Fig. 3.

4. Results

The ECC injection has been defined with a Dirac delta function lasting 10 s. Injection is performed at the start of the simulation (5 s). Consequently, the fastest transients appear in the first part of the simulations. Because of this, in the upcoming sections, only the initial 75 s will be shown, thus easing the result comparison.

4.1. Initial conditions

Initial conditions are assessed for the boundary BC_1 and BC_2 sets and k-ε turbulence model. This approach mitigates the variances different turbulent models might introduce, while also providing insight into BC associated disparities for cases with same initial conditions. Presented results reflect the IC introduced variances and do not represent the final simulation. BC_3 set has been excluded to simplify the comparison. Concentrations in points 1–4 for both cold start and warm start are given in Fig. 4.

It is evident that initial conditions have an influence on overall results, with absolute differences in concentrations of up to 0.05 in the CL (points 1–2) and parts of the core, depending on the IC. Concentration levels in the upper and lower DC reveal higher IC associated deviations. Relative discrepancies between setups can reach 100%. Overall, meaningfully more accurate results are observed for cold start and BC_2. Measurements in the core reveal similar trends. Significant concentration discrepancy is observed in point 5. These errors can partially be attributed to the numerical round-off. Furthermore, due to long travel distance, tracer concentrations in core are lower. Therefore, even for small disparities, relative errors are high. Additional tests using the RSM model exhibited marginal improvements. In the upcoming analyses warm start IC will be used since the results correspond to the measured values more closely.

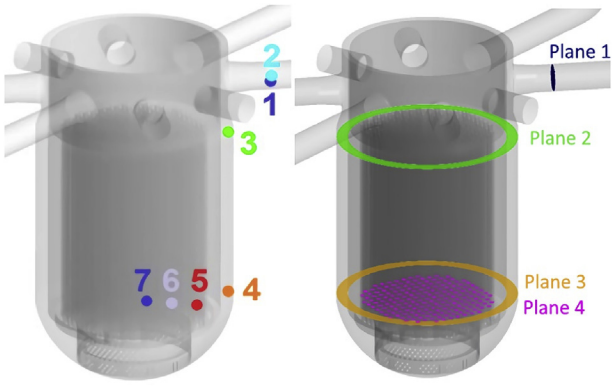

Fig. 3. Measurement points and planes.

4.2. Boundary conditions

Boundary conditions are analyzed in a series of simulations where warm start and k-ε turbulence model are fixed parameters. For BC_3, the HL_1 was slightly extruded in order to stabilize the flow. This modification has had no influence on resulting concentrations for this case. Streamlines in Fig. 5 depict flow patterns through the RPV. It is apparent that the fluid flows mostly around the core barrel and not directly through the downcomer. With inactive CL's modeled as outlets (BC_1) most of the water circumvents the core. Only a minor percentage of the total flow goes through the HL. When kept closed (BC_2, BC_3), fluid exits through the HL's in its entirety. Significant differences between BC_2 and BC_3 are observed on the core outlet. At the core level, velocities, and thus the flow for BC_1 case, are weak. This behavior is the result of previously mentioned circumvention through the CL's. On average, BC_3 has the highest core flow while BC_2 demonstrates intensive flow on the core perimeter. According to results and recommendations, BC_3 is the only appropriate and thus adopted boundary condition.

4.3. Turbulence modelling

Marginal differences between measured concentrations in points 1 and 2 and experimental results have thus far been demonstrated. Presented results for k-ε model are representative of other turbulence models as well. It is sensible to assume that agreement in these points is a consequence of insufficient distance between ECC nozzle and measurement points. General point proximity also affects the results and might lead to erroneous conclusions. Concentrations (temperature) in the downcomer are responsible for the PTS scenario and should be in focus. Results in measurement planes contribute scantly to overall understanding of the flow due to spatial averaging.

Realizable k-ε model, though evaluated, showed no improvements over the standard k-ε model. Discrepancy was below 0.5%. Consequently, these results have been disregarded. k-ε model produces compelling results whereas SST k-ω undeniably underpredicts concentrations with errors occasionally above 100%. Errors can be partially attributed to the maintained $y^+ = 30$ range. On the other hand, SST model should be able to account for this by utilizing the k-ε switch in the free flow, which is not the case. Discrepancies can therefore be attributed to both grid inadequacy for the given model as well as challenging transition gradients which affect the accuracy of the SST k-ω. It is evident that for SST k-ω lower y^+ values should be utilized, which impacts the overall computational efficiency. When compared to k-ε and RSM, k-ω and SST variant are worse. This observation holds true in points 5, 6 and 7. Disparities can primarily be attributed to numerical errors which, at lower concentrations typical of points 5, 6 and 7, can lead to significant relative errors. Noted maxima values further emphasize differences between turbulence models. Overall, standard k-ε model produces best predictions, both in terms of values and trendlines, with an apparent tendency to overestimate the concentrations. From a safety standpoint, this is desirable. Conservative values entail sturdier and more reliable designs. This is not to say that k-ε model is superior, however, for this type of a problem and chosen approach it is highly reliable.

4.4. Time step and inner iterations

Time step refinement has been done to achieve a balance between computational time and accuracy. Value used in past simulations, $t_s = \frac{1}{64}s$, is a best estimate from a series of successive simulations using k-ε model and BC_3 from warm start. During the initial 5 s, 10 inner iterations has been enforced, followed by 20

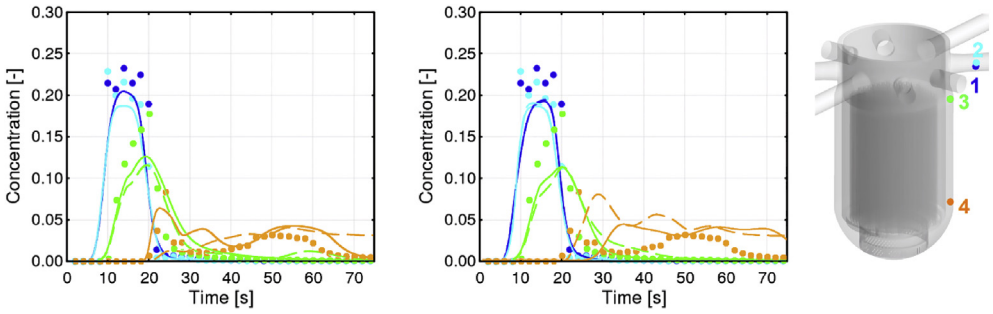

Fig. 4. Tracer concentrations in measurement points 1–4 for simulations from cold start (left) and warm start (right). Points represent experimental data, dashed lines simulations with BC_1, continuous lines simulations with BC_2.

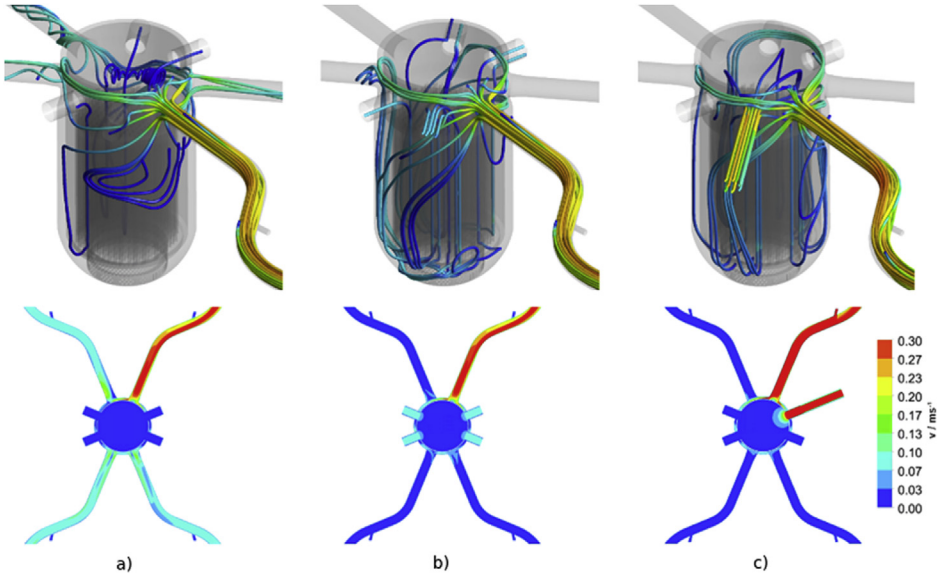

Fig. 5. Flow patterns through the RPV and values at the HL plane: a) BC_1, b) BC_2, c) BC_3.

during the next 20 s (injection) and finally ending with 10 iterations until simulation termination. Initial improvement incorporates reduced time step, $t_s = \frac{1}{128}s$, with halved inner iterations during the entire simulation, thus utilizing the same combined number of iterations. This approach yielded results with negligible differences and is therefore adopted due to beneficial lower time stepping which could provide better insight into fast-paced mixing phenomena. Further reductions were deemed unnecessary.

In an attempt to reduce simulation time and computational cost three distinct cases with reduced number of iterations have been additionally defined:

- Case 1: [0,5) s - 5 iterations; [5,25) s - 10 iterations; [25,300] s - 5 iterations
- Case 2: 5 iterations throughout the simulation
- Case 3: 3 iterations throughout the simulation

Results show that there is no difference between cases 1 and 2 as the solution reaches stable convergence levels with equal concentration in both scenarios. Further reduction (Case 3) leads to significant deviations in concentration values. These values are a direct consequence of incomplete convergence and are thus discarded. Simulations indicate that 5 iterations throughout is sufficient to achieve satisfactory results.

4.5. Best estimate

Findings outlined in previous sections are implemented in a best-estimate simulation. Essential settings include k-ε turbulence model, 5 inner iterations and a time step $t_s = \frac{1}{128}s$. Flow is analyzed from warm start with applied BC_3 boundary conditions set, thus forcing the fluid to move through a single inlet and outlet. Simulation was conducted on a 60 core AMD Opteron 6386SE server with a total computational time of 173 h.

Due to overall complexity and time-associated instability of the flow, leading to tracer concentration fluctuations, it is challenging to qualitatively quantify and validate concentrations in specific measurement locations. Seven distinct points have however been chosen, each corresponding to a single measurement point in the wire-mesh sensors. Time evolution of concentrations in these points is given in Fig. 6.

Measurement points 1 and 2 are representative of the reactor inlet sensor. Point 1 is close to the wall and at the maximum overestimates the concentration by approximately 0.04. This disparity can be partially attributed to unresolved wall-bounded flow. At point 2 results are mostly in accordance with the experimental data; concentrations differ by ±0.01. Values in UDC and LDC are similarly acceptable. At worst, they underestimate the tracer concentrations by 0.025. Values at the core inlet, represented by

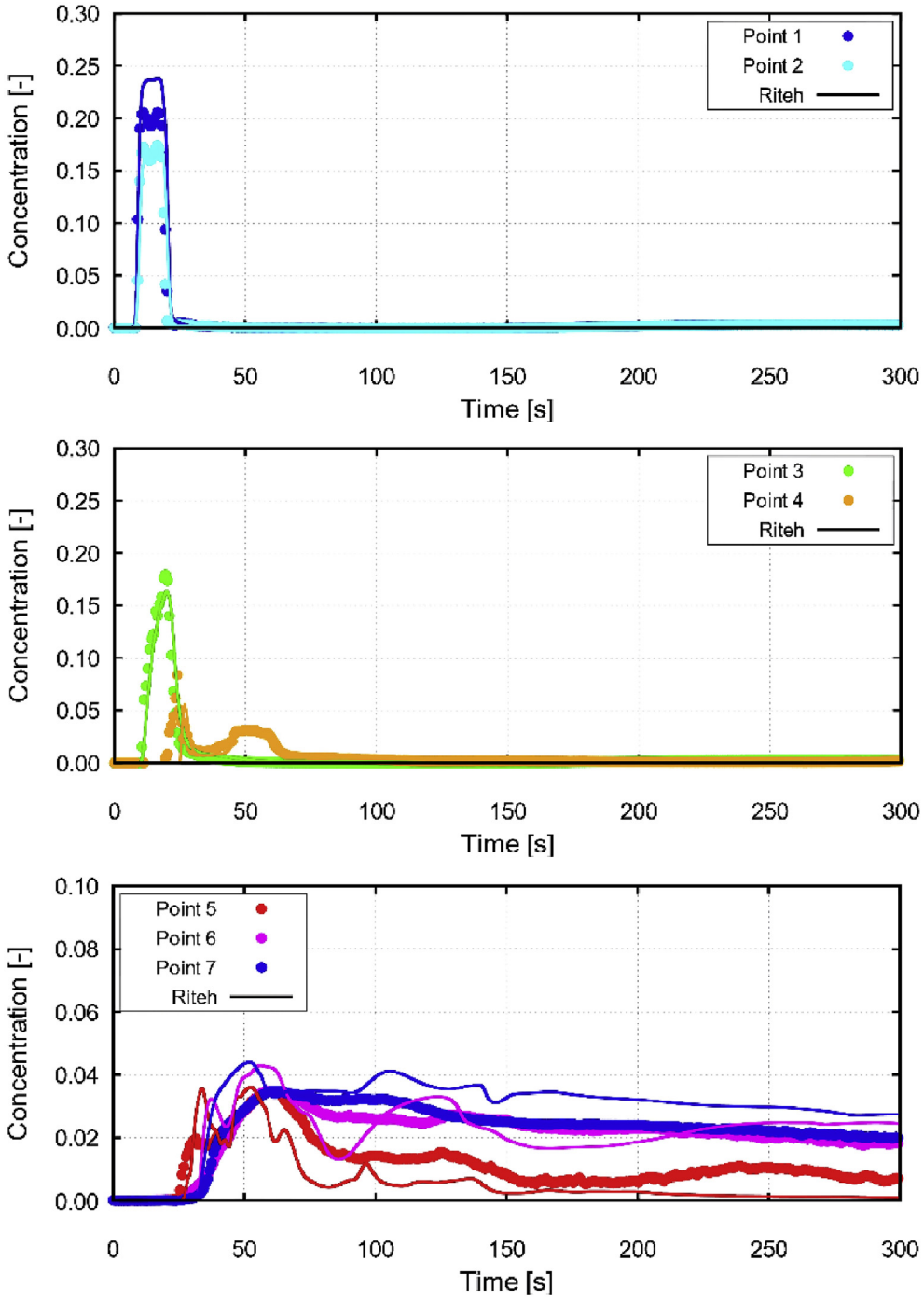

Fig. 6. Tracer concentrations in measurement points 1–7 for best estimate case. Points represent experimental data, continuous line simulation results.

point 5–7, show larger deviations, mainly due to lower absolute concentrations. Overall, errors are around 0.01.

Perturbation at measurement points is expected. This behavior can be accounted for by employing spatial averaging across all measurement points. Time-dependent spatially averaged concentrations can be calculated according to (3):

$$\overline{C} = \frac{1}{N}\sum_{i=1}^{N} C_i \tag{3}$$

where C_i is concentration at a point, N number of measurement points and $\overline{C}$ spatially averaged concentration. Spatially averaged values in measurement planes 1–4 match the trendlines and show reasonable agreement with the experimental data. Values in CL_1 and core inlet are slightly overpredicted and differ at worst by 0.02. Throughout the UDC and LDC, errors are marginal and below 0.01. Averaged results are shown in Fig. 7. Local concentration maxima values are interesting from a safety standpoint; they represent areas with potentially highest temperature. Maximum concentration values at sensor locations can be determined by filtering the results for every measurement point according to (4):

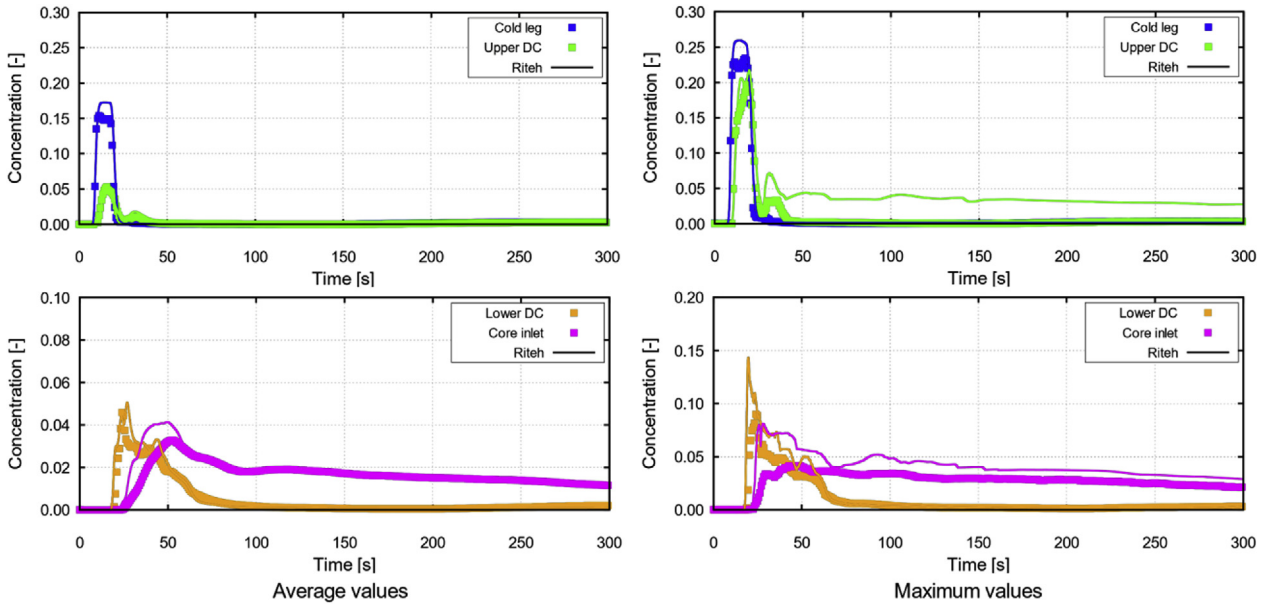

Fig. 7. Spatially averaged tracer concentrations in measurement planes (left) and maximum noted values (right) for best estimate case. Points represent experimental data, continuous line simulation results.

$$C_{max} = \max(C_1 \ldots C_i), \quad i = 1 \ldots N \tag{4}$$

Based on results presented in Fig. 7, it is clear that time-evolution of local maxima overpredicts concentrations at all locations. This is desirable as it leads to more durable reactor design.

Contour plots of tracer concentrations at key measurement planes are shown in Fig. 8. Displayed time-dependent results describe the flow through the DC and the core. It is evident that after 20 s tracer fluid has not yet reached the core. Reduction of the tracer concentration in the UDC can be attributed to the mixing of the tracer. After 30 s sharp drop in concentrations in the UDC has been detected. This result is a consequence of the tracer leaving the UDC. Maximum concentration in the core and LDC has remained unchanged. After 45 s concentration in the UDC dropped to 0. Both in the core and LDC, residual tracer concentrations have been found even after 60 s. These concentrations persisted throughout the simulation.

5. Conclusion

Results presented in this work demonstrate the importance of proper boundary conditions, initial conditions and overall simulation settings, and their influence on the outcome of a buoyancy driven mixing simulation in the ROCOM facility. It is obvious and clearly shown that each of these components plays a vital role in the quality and accuracy of the final solution.

Numerical grid used in this study offered good convergence, consequently, further improvements were not feasible due to computational requirements and sheer scope of work. Therefore, grid dependence and grid refinement study, especially in key areas, as well as boundary layer solving up to the wall, rather than modelling, should be a focus of novel studies. For presented case, k-ε model produces best overall results. Alternatives, such as k-ω model, show strength in some measurement locations (LDC, core inlet) and are invaluable for wall-bounded flows.

Summary findings are evaluated in a best-estimate case. Trendlines are well represented whereas conservative results in the DC could be improved. Local perturbations in distinct measurement points in a worst-case scenario overpredict the tracer concentrations by 0.04 at the inlet sensor. Errors in concentrations increased as the flow developed, with highest discrepancies at the core inlet. If perturbations are accounted for by employing averaging of the time-evaluated concentrations at the measurement points, concentrations differ by 0.01 on average. Concentration maxima at the

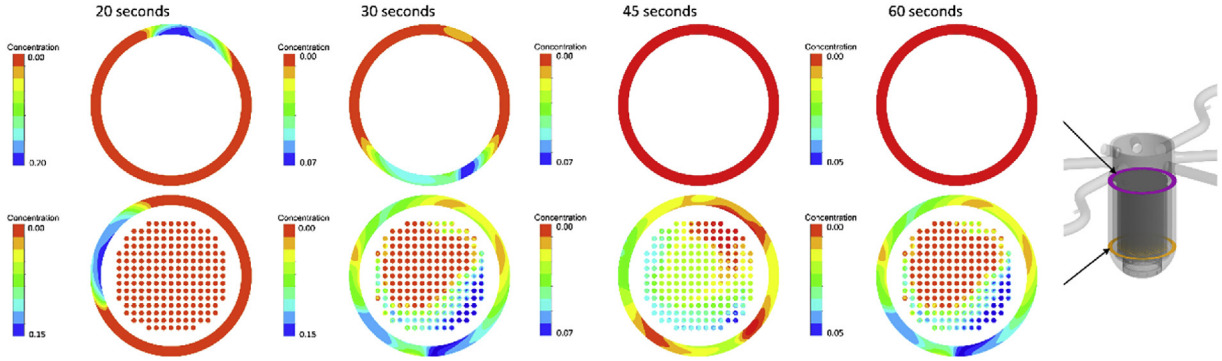

Fig. 8. Tracer concentrations in UDC (top), LDC and core inlet (bottom). Results are shown after 20s, 30s, 45s and 60s.

sensor locations across all measurement planes is overpredicted. These observations demonstrate that the chosen turbulence model underestimates the intensity of turbulent mixing. Noted overpredictions can also be attributed to the bypass effect, which, due to set boundary conditions, is negligible, and can therefore lead to increased concentrations. This is not to say the results are bad or undesirable, since from a safety perspective, they ensure reactor longevity.

On an absolute scale, the largest errors were below 5%, while at the core inlet, they are below 2% for the maximum and 1% for spatially averaged values. Given the differences in results when using different turbulent models and simulation settings, it is evident that the CFD results should not be taken as a definitive solution, but rather as a robust prediction. On the other hand, since time-evolution of concentration maxima is consistently overpredicted, whereas for spatial averaging results are mostly in accordance with the measurements, these two approaches could be utilized to assess the validity of the design as they introduce a "safety buffer" which should prevent incidents. For CFD to be used as an infallible prediction tool, further investigations on reactor mixing problems should be undertaken.

Compliance with ethics requirements

This article does not contain any studies with human or animal subjects.

Declaration of competing interest

The authors have declared no conflict of interest.

Appendix A. Supplementary data

Supplementary data related to this article can be found at https://doi.org/10.1016/j.net.2020.06.002.

References

[1] U. Rohde, S. Kliem, B. Hemström, T. Toppila, Y. Bezrukov, The European Project FLOMIX-R: Description of the Slug Mixing and Buoyancy Related Experiments at the Different Test Facilities (Final Report on WP 2), FZR, Forschungszentrum Rossendorf, 2005.

[2] V. Povarov, O. Urazov, M. Bakirov, V. Levchuk, Design and experimental assessment of thermal stratification effects on operational loading of surge line of Unit 5, Novovoronezh NPP, Nucl. Energy Technol. 3 (2) (2017) 92–97.

[3] U. Grundmann, U. Rohde, Investigations on a boron dilution accident for a VVER-440 type reactor by the help of the code DYN3D, in: ANS Topical Meeting on Advances in Reactor Physics, 1994.

[4] A. Martin, D. Alvarez, F. Cases, Three Dimensional Calculations of the Primary Coolant Flow in a 900 MW PWR Vessel. Steady State and Transients Computations, Electricite de France (EDF), 1996.

[5] F. Alavyoon, B. Hemström, N. Andersson, R. Karlsson, Experimental and Computational Approach to Investigating Rapid Boron Dilution Transients in PWRs, OECD, 1996.

[6] T. Höhne, U. Rohde, S. Kliem, T. Toppila, J. Elter, J. Remis, J. Klepac, I. Farkas, T. Farkas, The European Project FLOMIX-R: Fluid Mixing and Flow Distribution in the Reactor Circuit: Final Summary Report, FZR, Forschungszentrum Rossendorf, 2005.

[7] S. Kliem, T. Sühnel, U. Rohde, T. Höhne, H.-M. Prasser, F.-P. Weiss, Experiments at the mixing test facility ROCOM for benchmarking of CFD codes, Nucl. Eng. Des. 238 (3) (2008) 566–576.

[8] S. Kliem, H.-M. Prasser, T. Sühnel, F.-P. Weiss, A. Hansen, Experimental determination of the boron concentration distribution in the primary circuit of a PWR after a postulated cold leg small break loss-of-coolant-accident with cold leg safety injection, Nucl. Eng. Des. 238 (7) (2008) 1788–1801.

[9] H.-M. Prasser, S. Kliem, Coolant mixing experiments in the upper plenum of the ROCOM test facility, Nucl. Eng. Des. 276 (2014) 30–42.

[10] H. Prasser, G. Grunwald, T. Hoehne, S. Kliem, U. Rohde, F. Weiss, Coolant Mixing in a PWR-de-Boration Transients, Steam Line Breaks And Emergency Core Cooling Injection-Experiments And Analyses, American Nuclear Society, 2002.

[11] U. Rohde, T. Höhne, S. Kliem, B. Hemström, J. Lillington, M. Scheuerer, T. Toppila, T. Dury, J. Remis, P. Muhlbauer, others, Fluid Mixing and Flow Distribution in the Reactor Circuit (FLOMIX-R), vol. 27, Institute of Safety Research, 2005.

[12] A. Schaffrath, K.-C. Fischer, T. Hahm, S. Wussow, Validation of the CFD code fluent by post-test calculation of a density-driven ROCOM experiment, Nucl. Eng. Des. 237 (15–17) (2007) 1899–1908.

[13] F. Moretti, D. Melideo, F. D'auria, T. Höhne, S. Kliem, CFX simulations of ROCOM slug mixing experiments, J. Power Energy Syst. 2 (2) (2008) 720–733.

[14] T. Höhne, S. Kliem, U. Bieder, Modeling of a buoyancy-driven flow experiment at the ROCOM test facility using the CFD codes CFX-5 and Trio_U, Nucl. Eng. Des. 236 (12) (2006) 1309–1325.

[15] T. Höhne, S. Kliem, U. Rohde, F.-P. Weiss, Modeling of buoyancy-driven flow experiment at the Rocom test facility using the CFD-code Ansys CFX, Int. J. Nucl. Power 3 (2007) 168–174.

[16] M. Labois, J. Panyasantisuk, T. Höhne, S. Kliem, D. Lakehal, On the prediction of boron dilution using the CMFD code TRANSAT: the ROCOM test case, in: Proceedings of the CFD for Nuclear Reactor Safety Applications, CFD4NRS-3) Workshop, 2012.

[17] Y.-J. Cho, H.-Y. Yoon, Numerical analysis of the ROCOM boron dilution benchmark experiment using the CUPID code, Nucl. Eng. Des. 341 (2019) 167–175.

[18] F. Moretti, Contribution to the Assessment of CFD Codes for in Vessel Flow Investigation, 2009. Pisa.

[19] M. Boumaza, F. Moretti, R. Dizene, Numerical simulation of flow and mixing in ROCOM facility using uniform and non-uniform inlet flow velocity profiles, Nucl. Eng. Des. 280 (2014) 362–371.

[20] Q. Feng, U. Bieder, T. Höhne, Analysis of buoyancy-driven flow in the ROCOM test facility, Energy Procedia 127 (2017) 44–53.

[21] T. Höhne, S. Kliem, U. Bieder, IAEA CRP benchmark of ROCOM PTS test case for the use of CFD in reactor design using the CFD-Codes ANSYS CFX and TrioCFD, Nucl. Eng. Des. 333 (2018) 161–180.

[22] R. Puragliesi, Assessment of a URANS CFD model for gravity driven flows: a comparison with OECD/PKL2 ROCOM experiments, Nucl. Eng. Des. 356 (2020).

[23] Ansys Inc., in: Ansys Fluent User Guide, Release, 16.2, Ansys, 2015.

[24] J.H. Ferziger, M. Peric, Computational Methods for Fluid Dynamics, Springer Science & Business Media, 2012.

[25] T. Hohne, Specification of the PTS Experiment D10m10, HZDR, Rossendorf, 2016.